Electronic supplementary information (ESI) for

Novel enantiomorphic Pb-coordination polymers dictated by the corresponding chiral ligands, [Pb((*R*,*R*)-*TBA*)(H_2O)]·1.7H_2O and [Pb((*S*,*S*)-*TBA*)(H_2O)]·1.7H_2O [*TBA* = 1,3,5-triazin-2(1H)-one-4,6-bis(alanyl)]

*Yunseung Kuk and Kang Min Ok**

Department of Chemistry, Sogang University, Seoul 04107, Republic of Korea

*E-mail: kmok@sogang.ac.kr

Contents

Figure S1. ^{1}H and ^{13}C NMR spectra for (a) (*S*,*S*)-*TBA* and (b) (R,R)-*TBA*.

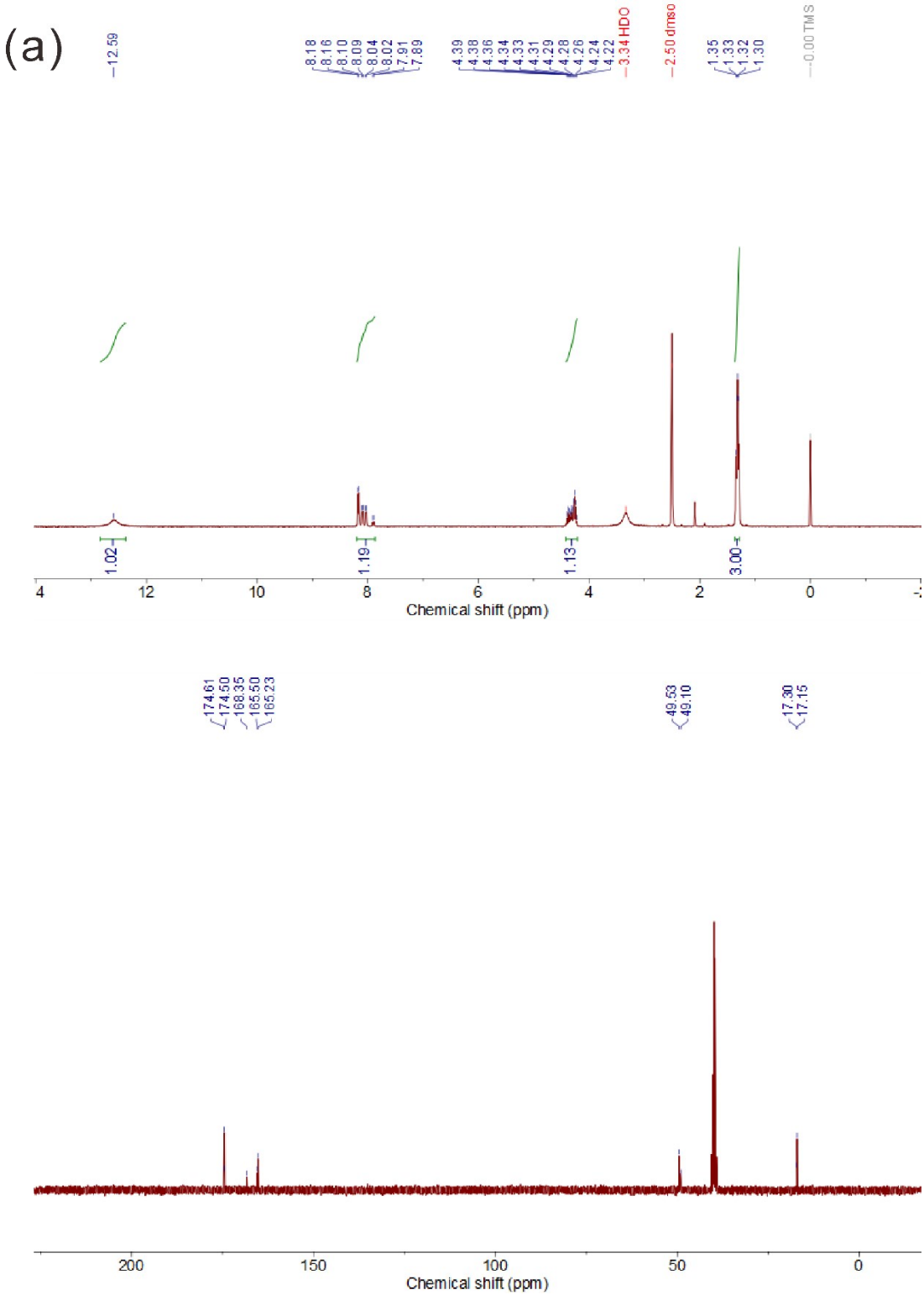

(b)

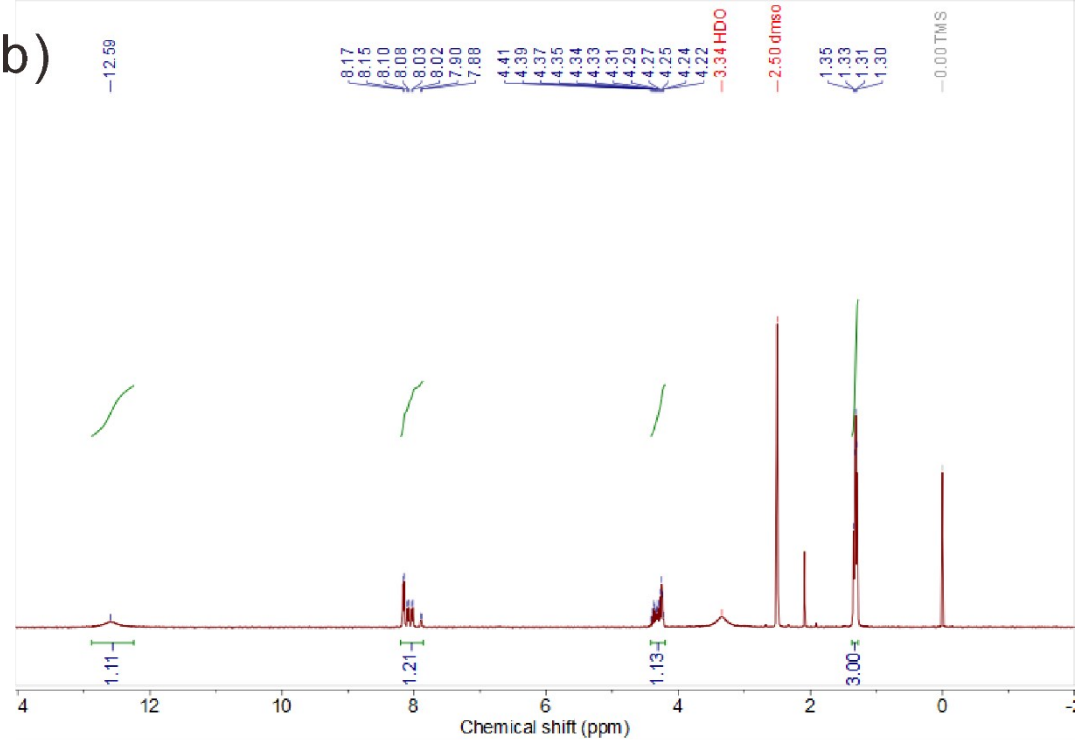
12.59
8.17
8.15
8.10
8.08
8.03
8.02
7.90
7.88
4.41
4.39
4.37
4.35
4.34
4.33
4.31
4.29
4.27
4.25
4.24
4.22
3.34 HDO
2.50 dmso
1.35
1.33
1.31
1.30
0.00 TMS
1.11
1.21
1.13
3.00
Chemical shift (ppm)

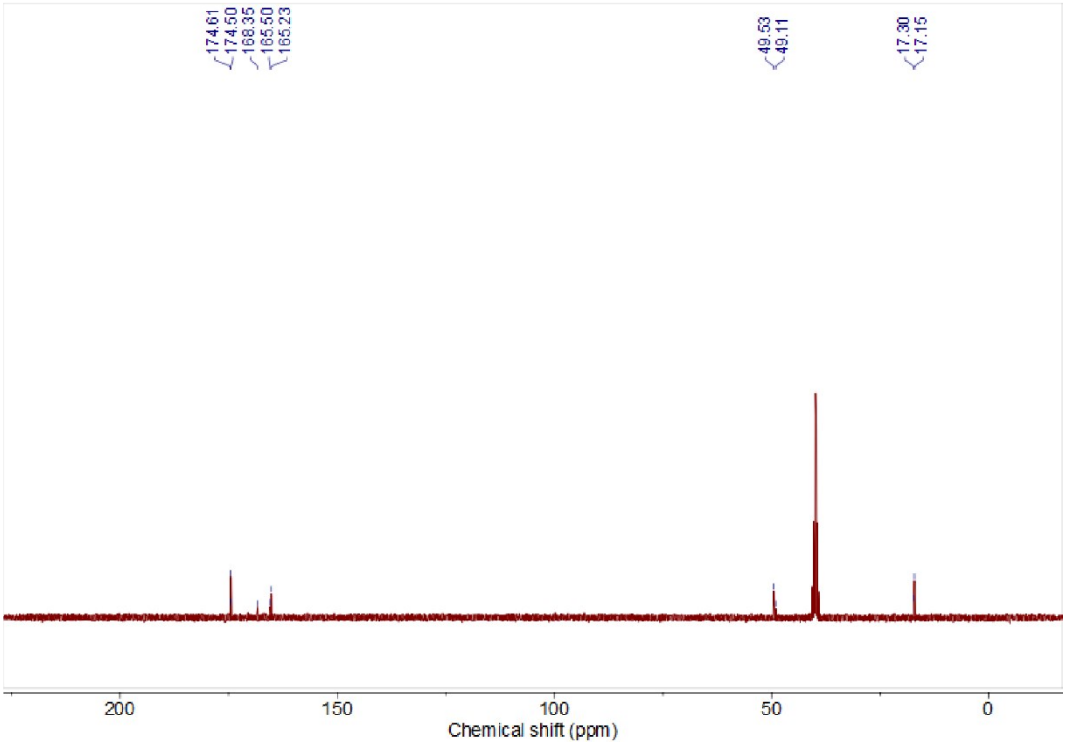
174.61
174.50
168.35
165.50
165.23
49.53
49.11
17.30
17.15
Chemical shift (ppm)

Figure S2. Ball-and-stick models of **R1** (left) and **S1** (right) in the *bc*-plane.

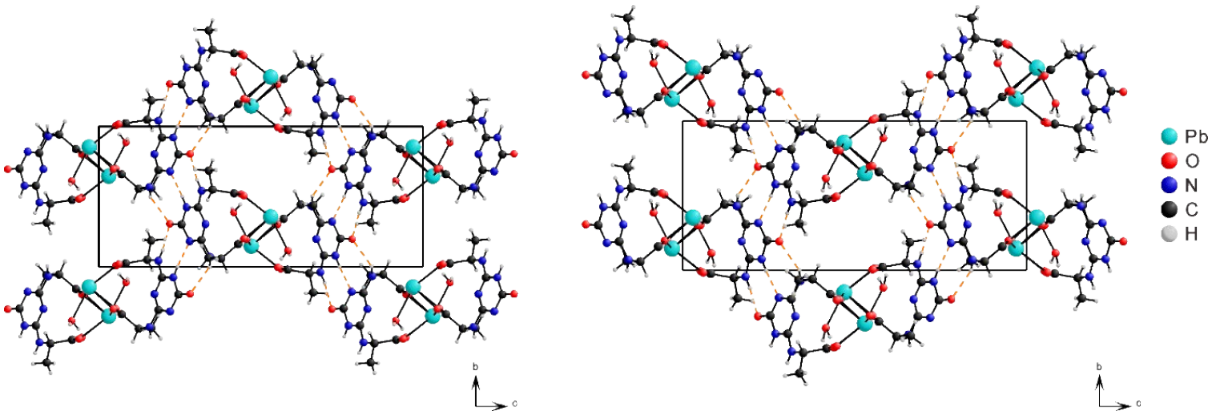

Figure S3. SEM-EDX data for **R1** and **S1**.

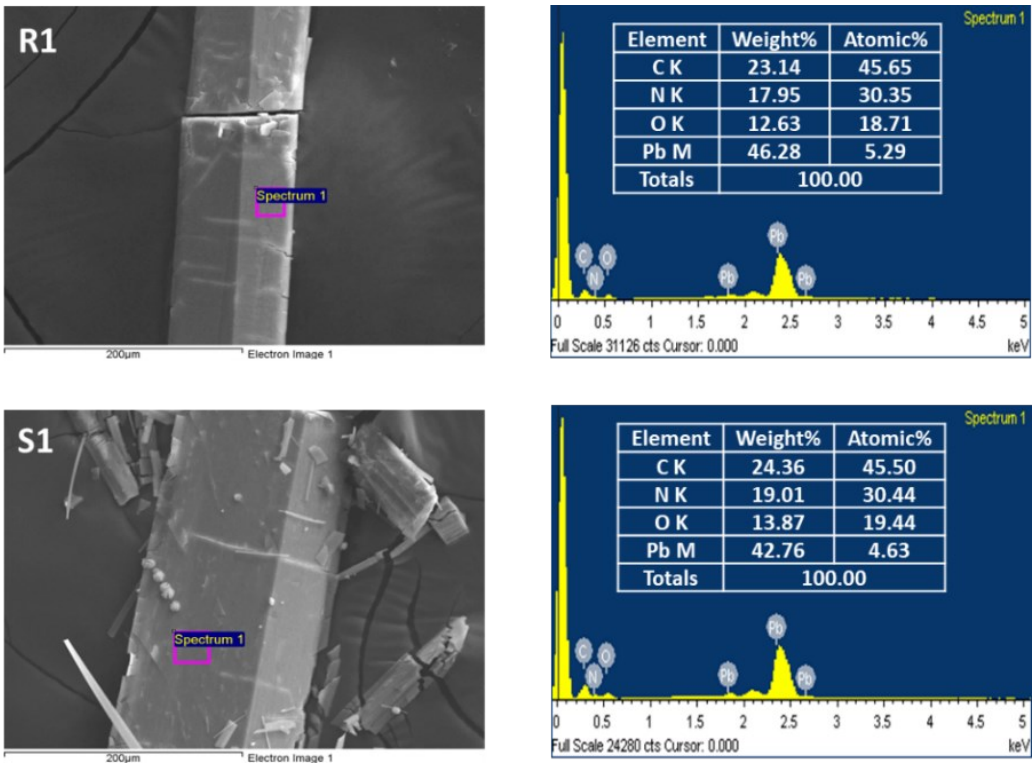

Figure S4. Calculated and experimental powder X-ray diffraction patterns for **R1** and **S1**.

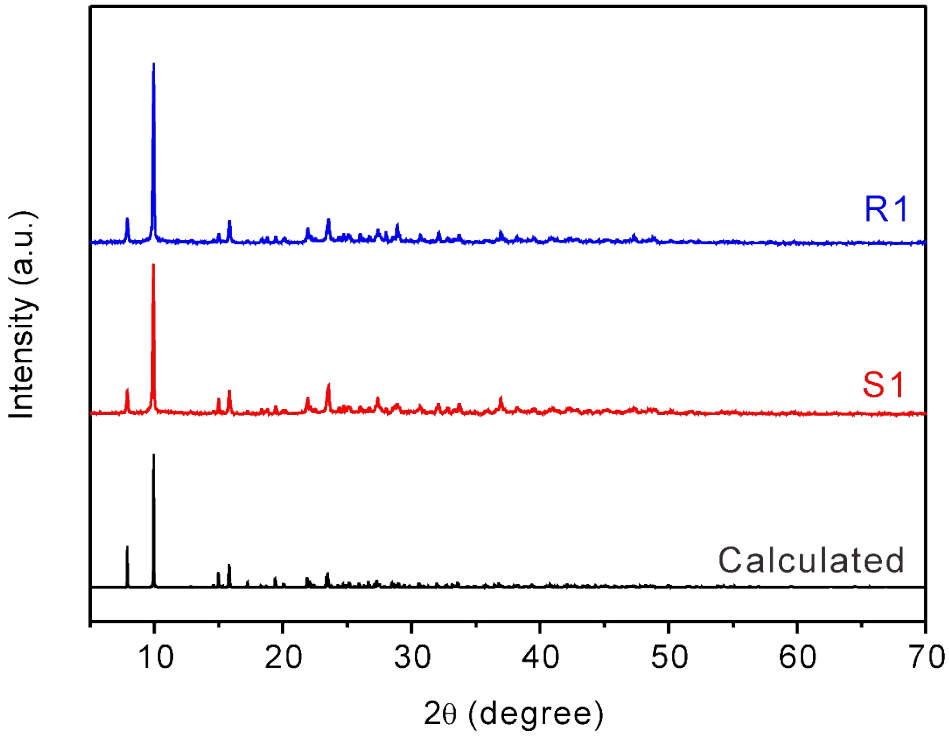

Figure S5. Infrared spectra for **R1**, **S1**, (*R*,*R*)-*TBA*, and (*S*,*S*)-*TBA*.

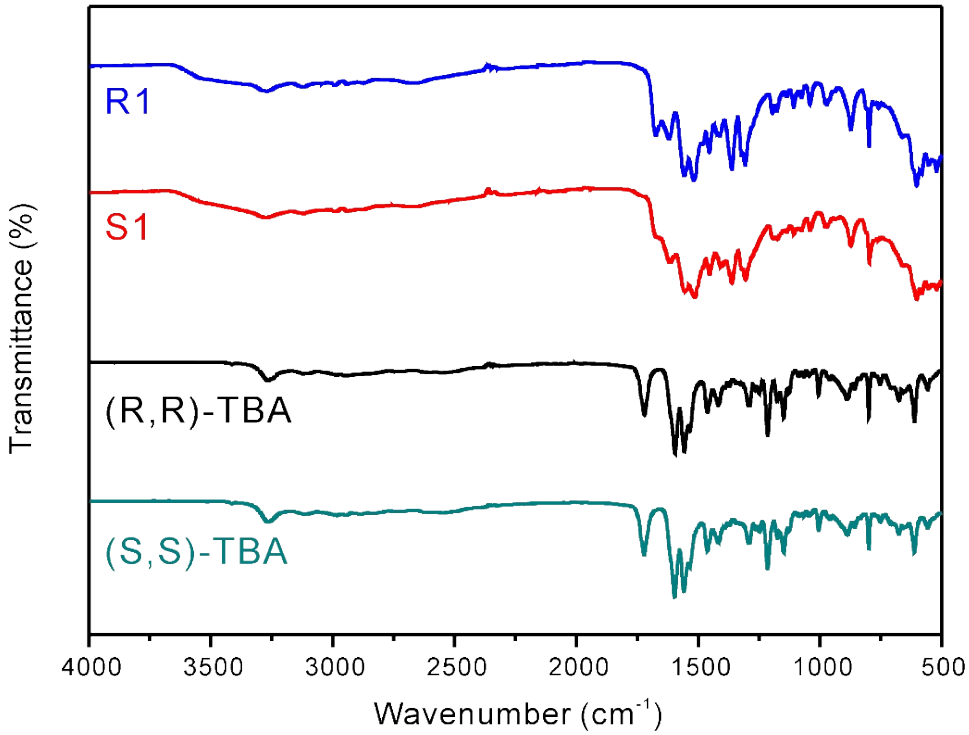

Figure S6. Thermogravimetric analysis diagrams and PXRD data at different temperatures for **R1** and **S1**.

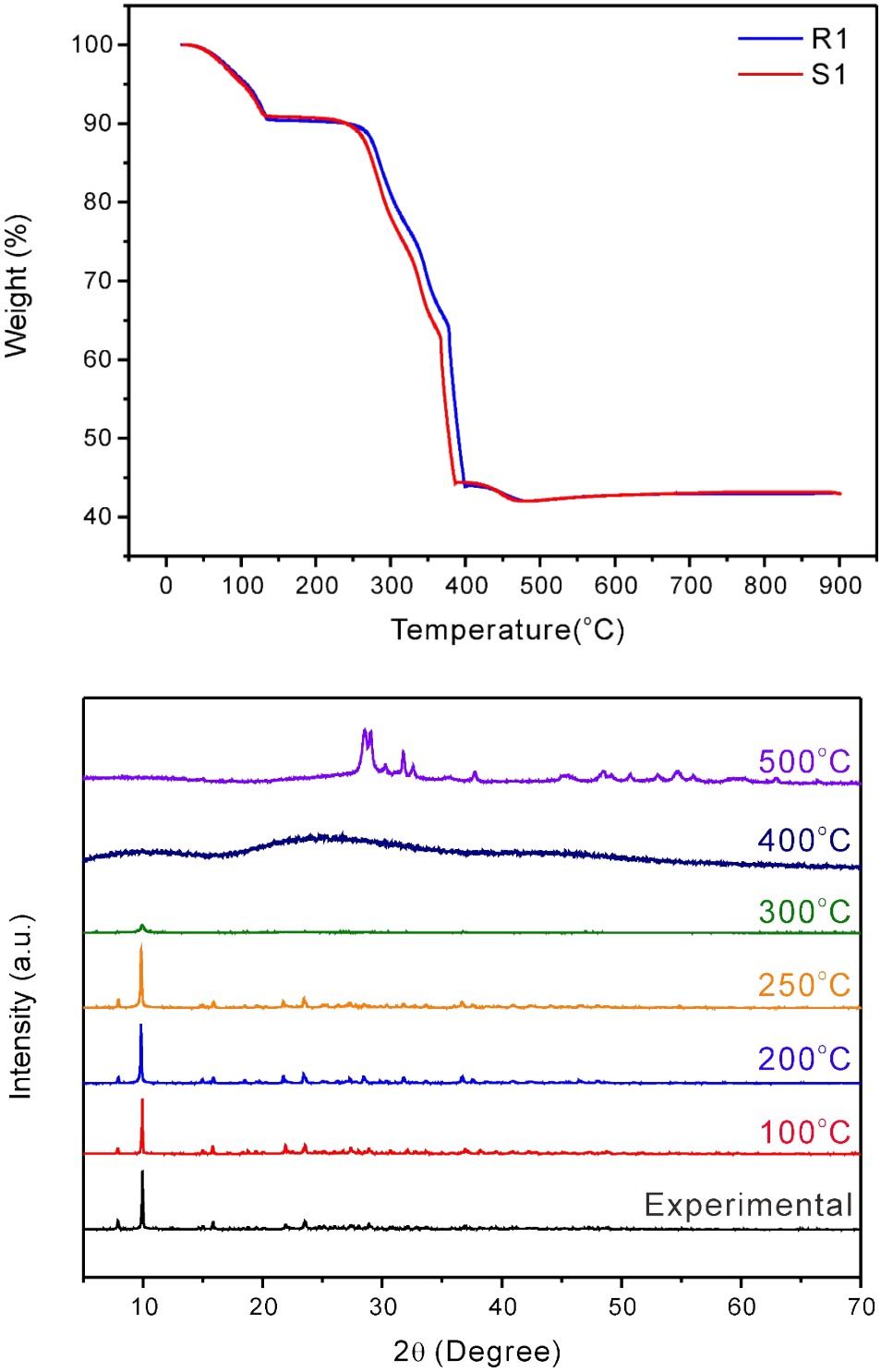

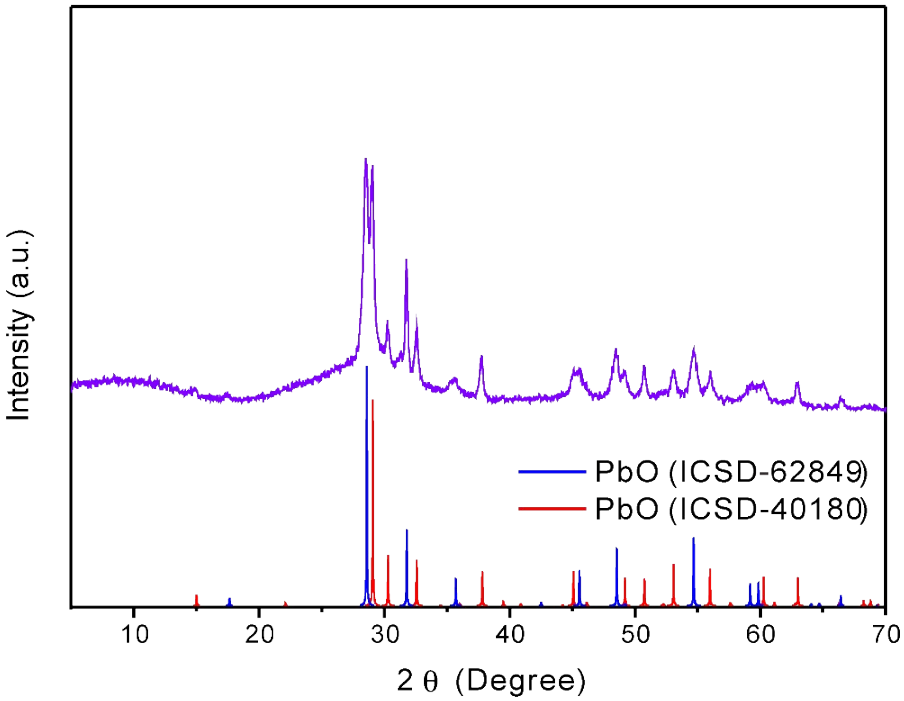
Intensity (a.u.)
PbO (ICSD-62849)
PbO (ICSD-40180)
10
20
30
40
50
60
70
2 θ (Degree)

Figure S7. UV-vis spectra for **R1**, **S1**, (*R*,*R*)-*TBA*, and (*S*,*S*)-*TBA*.

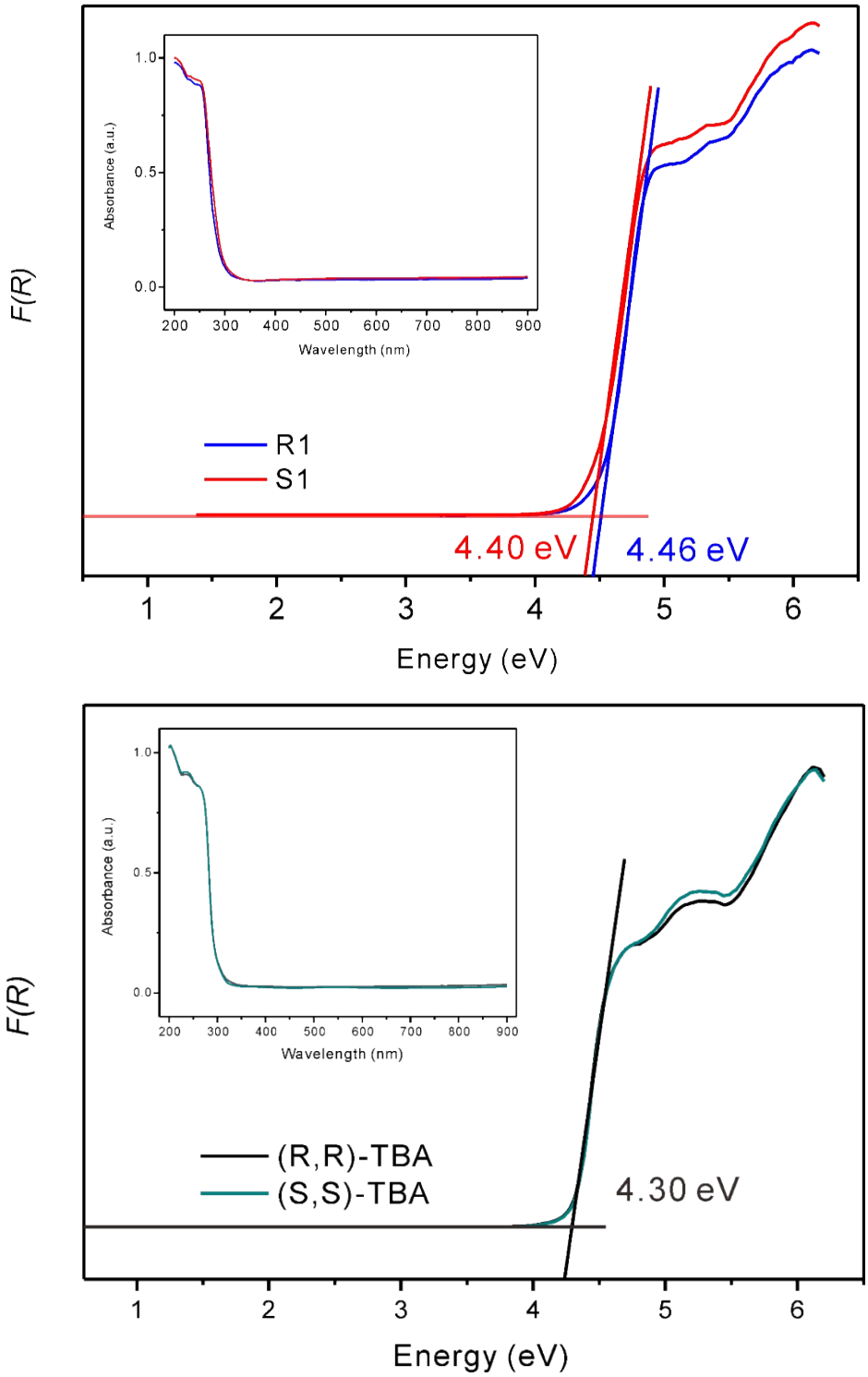

Figure S8. Partial density of state (PDOS) calculations of (a) **R1** and (b) **S1**. The Fermi level is represented at 0 eV.

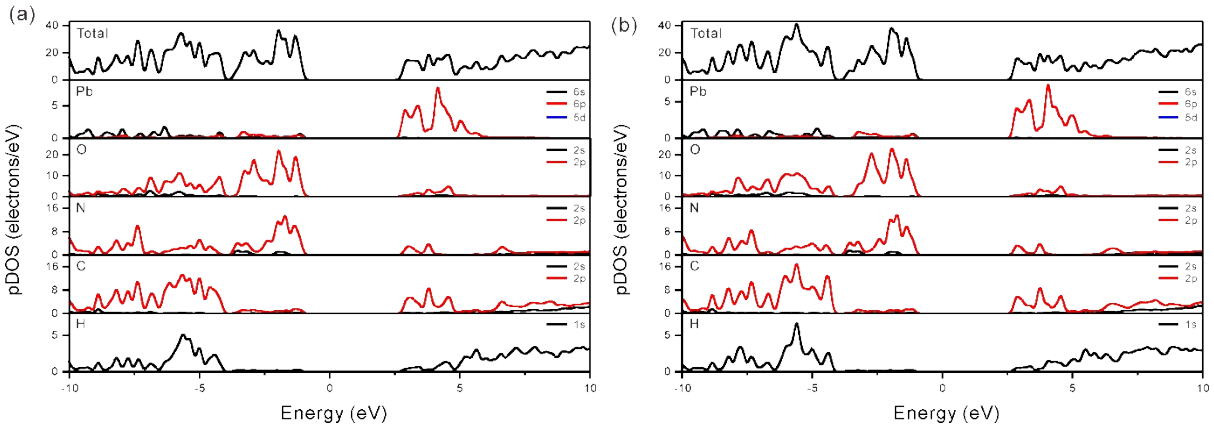

Figure S9. Gas adsorption isotherms of N_2 (blue) and CO_2 (red) on **S1** and PXRD patterns for **S1** after the degassing process.

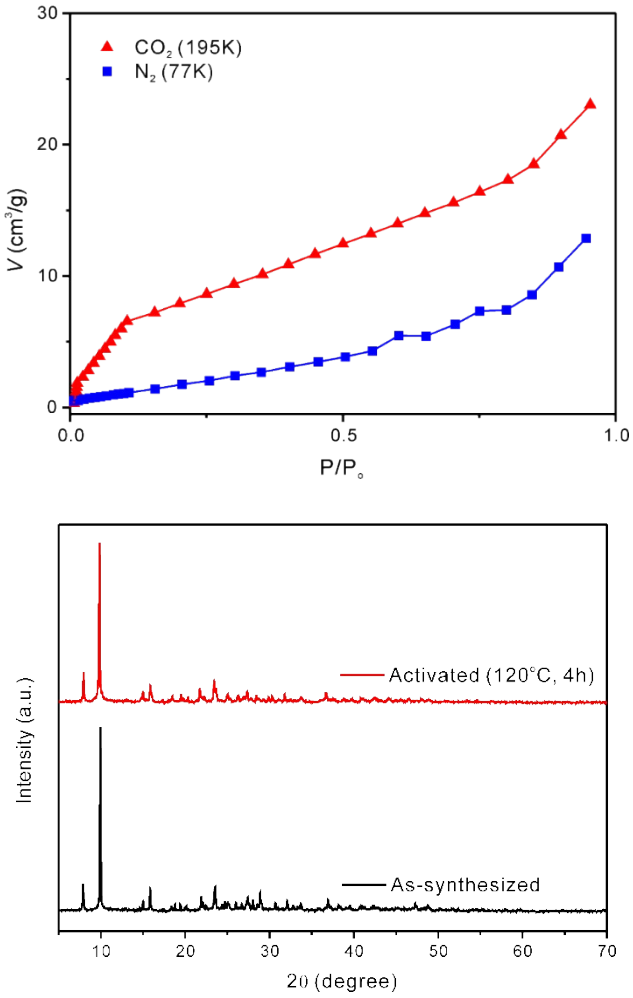

Figure S10. PXRD patterns after immersion into the (a) H_2SO_4 (pH = 0) and (b) KOH (pH = 14) solutions.

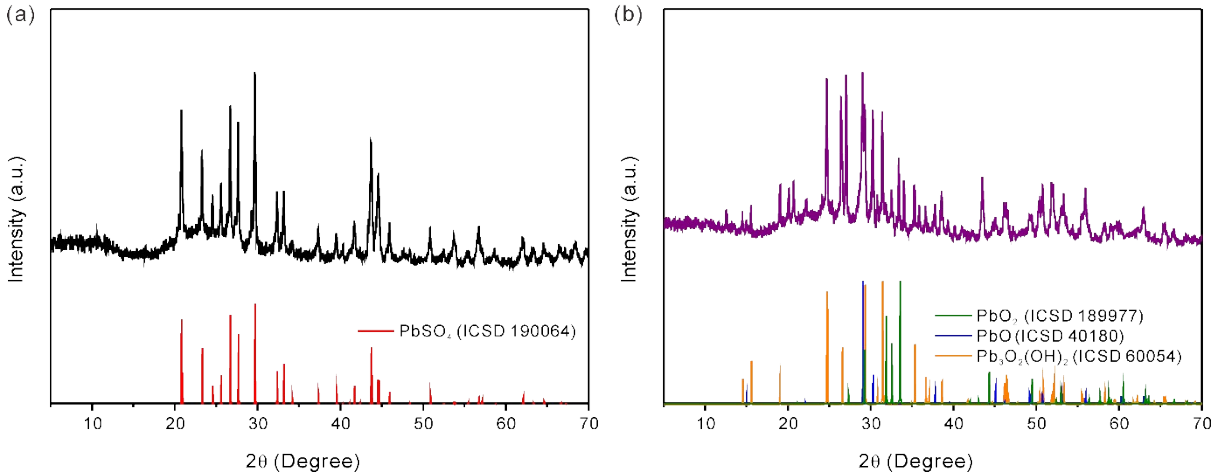

Figure S11. UV-vis spectra of CR dye solutions and adsorption maximum capacity (q_{max}).

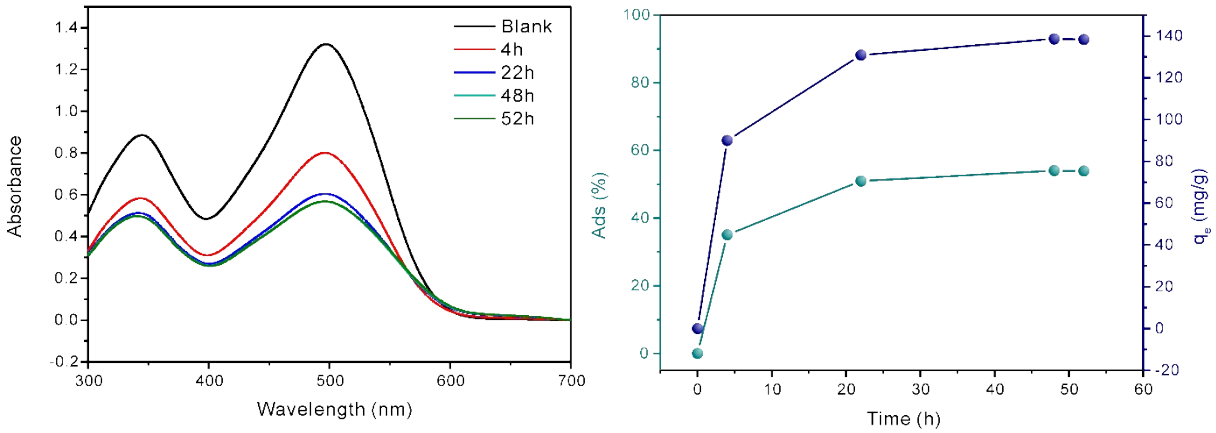

Figure S12. Congo red (CR), indigo carmine (IC), methyl orange (MO), and rhodamine B (RhB) structure and ball-and-stick model (light yellow, Na^+; green, Cl^-; black, C; blue, N; red, O; yellow, S; white, H).

Name	Structure	Ball-and-stick model
CR	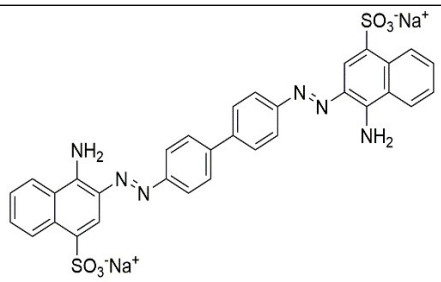	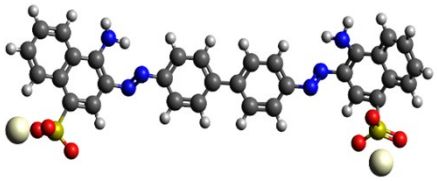
IC	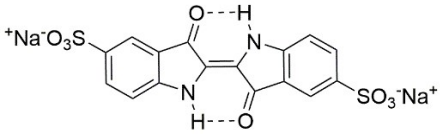	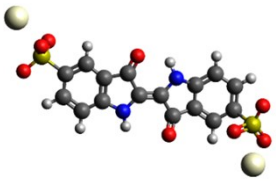
MO	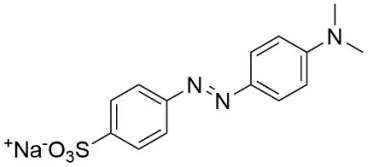	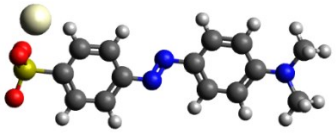
RhB	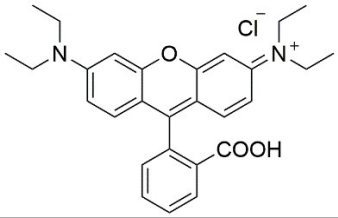	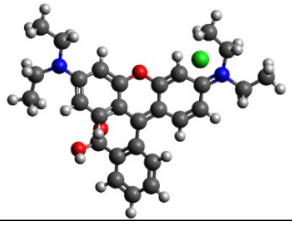

Figure S13. UV-vis spectra of (a) MO, (b) RhB, and (c) IC dye solutions.

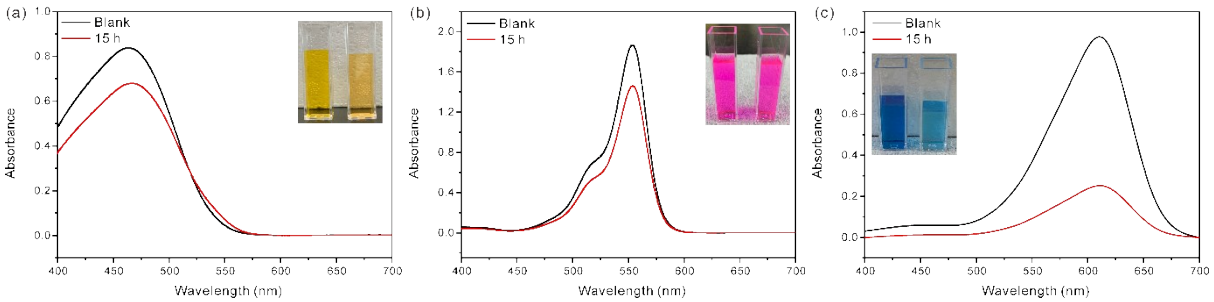

Figure S14. UV-vis spectra for CR solutions (a) at various particle sizes, (b) at pH 2, 3, and (c) 4, 5, 7, and 11.

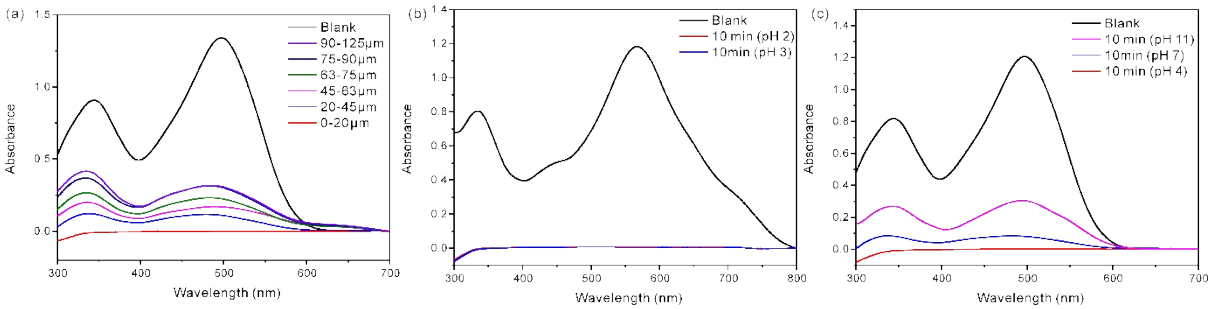

Table S1. Bond lengths [Å] and angles [°] for **R1**.

Selected bond distances (Å)			
Pb(1)–O(2)#1	2.495(7)	N(1)–C(3)	1.339(10)
Pb(1)–O(2)	2.518(7)	N(2)–C(1)	1.359(11)
Pb(1)–O(1)	2.558(8)	N(2)–C(2)	1.373(12)
Pb(1)–O(5)	2.597(8)	N(3)–C(3)	1.343(10)
Pb(1)–O(3)	2.606(10)	N(3)–C(2)	1.352(11)
Pb(1)–O(1)#2	2.697(8)	N(4)–C(3)	1.363(11)
Pb(1)–O(4)	2.795(10)	N(4)–C(4)	1.453(11)
O(1)–C(8)	1.233(11)	N(5)–C(1)	1.325(11)
O(2)–C(8)	1.239(10)	N(5)–C(5)	1.460(11)
O(3)–C(9)	1.248(13)	C(4)–C(6)	1.520(14)
O(4)–C(9)	1.241(13)	C(4)–C(8)	1.531(11)
O(6)–C(2)	1.242(12)	C(5)–C(7)	1.491(14)
N(1)–C(1)	1.334(11)	C(5)–C(9)	1.513(13)
Selected bond angle (°)			
O(2)#1–Pb(1)–O(2)	114.31(15)	C(9)–O(4)–Pb(1)	87.1(6)
O(2)#1–Pb(1)–O(1)	66.7(2)	C(1)–N(1)–C(3)	114.8(7)
O(2)–Pb(1)–O(1)	49.9(2)	C(1)–N(2)–C(2)	121.3(7)
O(2)#1–Pb(1)–O(5)	76.7(2)	C(3)–N(3)–C(2)	116.3(7)
O(2)–Pb(1)–O(5)	76.6(2)	C(3)–N(4)–C(4)	122.8(7)
O(1)–Pb(1)–O(5)	79.2(3)	C(1)–N(5)–C(5)	122.3(7)
O(2)#1–Pb(1)–O(3)	77.3(2)	N(5)–C(1)–N(1)	119.9(8)
O(2)–Pb(1)–O(3)	94.0(3)	N(5)–C(1)–N(2)	118.9(8)
O(1)–Pb(1)–O(3)	69.8(3)	N(1)–C(1)–N(2)	121.2(8)
O(5)–Pb(1)–O(3)	145.5(3)	O(6)–C(2)–N(3)	122.7(8)
O(2)#1–Pb(1)–O(1)#2	151.7(3)	O(6)–C(2)–N(2)	118.9(8)
O(2)–Pb(1)–O(1)#2	64.3(2)	N(3)–C(2)–N(2)	118.4(8)
O(1)–Pb(1)–O(1)#2	113.13(19)	N(1)–C(3)–N(3)	127.7(7)
O(5)–Pb(1)–O(1)#2	75.6(3)	N(1)–C(3)–N(4)	116.5(7)
O(3)–Pb(1)–O(1)#2	130.3(3)	N(3)–C(3)–N(4)	115.8(7)
O(2)#1–Pb(1)–O(4)	124.9(2)	N(4)–C(4)–C(6)	113.8(8)
O(2)–Pb(1)–O(4)	71.6(2)	N(4)–C(4)–C(8)	112.0(7)
O(1)–Pb(1)–O(4)	87.1(3)	C(6)–C(4)–C(8)	112.2(8)
O(5)–Pb(1)–O(4)	147.0(3)	N(5)–C(5)–C(7)	109.4(9)
O(3)–Pb(1)–O(4)	47.7(2)	N(5)–C(5)–C(9)	112.2(8)
O(1)#2–Pb(1)–O(4)	82.6(3)	C(7)–C(5)–C(9)	111.8(9)
C(8)–O(1)–Pb(1)	94.0(5)	O(1)–C(8)–O(2)	120.2(7)
C(8)–O(1)–Pb(1)#1	150.0(7)	O(1)–C(8)–C(4)	119.0(8)
Pb(1)–O(1)–Pb(1)#1	110.3(3)	O(2)–C(8)–C(4)	120.6(7)
C(8)–O(2)–Pb(1)#2	144.6(6)	O(4)–C(9)–O(3)	123.5(9)
C(8)–O(2)–Pb(1)	95.8(5)	O(4)–C(9)–C(5)	121.0(9)
Pb(1)#2–O(2)–Pb(1)	118.7(3)	O(3)–C(9)–C(5)	115.5(9)
C(9)–O(3)–Pb(1)	95.8(7)		
Symmetry operation : #1 x–1/2,–y+1/2,–z+1 #2 x+1/2,–y+1/2,–z+1			

Table S2. Bond lengths [Å] and angles [°] for **S1**.

Selected bond distances (Å)			
Pb(1)–O(1)#1	2.516(7)	N(1)–C(3)	1.344(13)
Pb(1)–O(1)	2.532(8)	N(2)–C(1)	1.368(12)
Pb(1)–O(2)	2.575(8)	N(2)–C(2)	1.388(13)
Pb(1)–O(5)	2.599(9)	N(3)–C(2)	1.353(13)
Pb(1)–O(4)	2.617(11)	N(3)–C(3)	1.361(12)
Pb(1)–O(2)#2	2.713(8)	N(4)–C(3)	1.378(13)
Pb(1)–O(3)	2.774(10)	N(4)–C(4)	1.461(12)
O(1)–C(8)	1.255(12)	N(5)–C(1)	1.326(13)
O(2)–C(8)	1.242(12)	N(5)–C(5)	1.457(13)
O(3)–C(9)	1.249(15)	C(4)–C(8)	1.516(13)
O(4)–C(9)	1.249(14)	C(4)–C(6)	1.549(15)
O(6)–C(2)	1.250(13)	C(5)–C(7)	1.507(17)
N(1)–C(1)	1.328(13)	C(5)–C(9)	1.553(15)
Selected bond angle (°)			
O(1)#1–Pb(1)–O(1)	114.23(16)	C(9)–O(4)–Pb(1)	94.8(7)
O(1)#1–Pb(1)–O(2)	66.5(2)	C(1)–N(1)–C(3)	115.4(8)
O(1)–Pb(1)–O(2)	49.9(2)	C(1)–N(2)–C(2)	120.7(9)
O(1)#1–Pb(1)–O(5)	76.5(3)	C(2)–N(3)–C(3)	116.2(9)
O(1)–Pb(1)–O(5)	76.9(3)	C(3)–N(4)–C(4)	122.6(9)
O(2)–Pb(1)–O(5)	79.1(3)	C(1)–N(5)–C(5)	122.0(9)
O(1)#1–Pb(1)–O(4)	77.5(3)	N(5)–C(1)–N(1)	120.4(9)
O(1)–Pb(1)–O(4)	94.0(3)	N(5)–C(1)–N(2)	118.1(9)
O(2)–Pb(1)–O(4)	70.2(3)	N(1)–C(1)–N(2)	121.5(9)
O(5)–Pb(1)–O(4)	145.7(3)	O(6)–C(2)–N(3)	122.6(10)
O(1)#1–Pb(1)–O(2)#2	151.9(3)	O(6)–C(2)–N(2)	118.7(10)
O(1)–Pb(1)–O(2)#2	64.2(2)	N(3)–C(2)–N(2)	118.7(9)
O(2)–Pb(1)–O(2)#2	113.07(19)	N(1)–C(3)–N(3)	127.1(9)
O(5)–Pb(1)–O(2)#2	75.9(3)	N(1)–C(3)–N(4)	117.7(8)
O(4)–Pb(1)–O(2)#2	130.0(3)	N(3)–C(3)–N(4)	115.2(9)
O(1)#1–Pb(1)–O(3)	125.5(2)	N(4)–C(4)–C(8)	113.2(8)
O(1)–Pb(1)–O(3)	71.5(3)	N(4)–C(4)–C(6)	111.9(9)
O(2)–Pb(1)–O(3)	87.8(3)	C(8)–C(4)–C(6)	112.5(10)
O(5)–Pb(1)–O(3)	147.0(3)	N(5)–C(5)–C(7)	110.4(10)
O(4)–Pb(1)–O(3)	48.2(2)	N(5)–C(5)–C(9)	112.1(9)
O(2)#2–Pb(1)–O(3)	81.8(3)	C(7)–C(5)–C(9)	111.6(10)
C(8)–O(1)–Pb(1)#2	144.0(7)	O(2)–C(8)–O(1)	119.4(8)
C(8)–O(1)–Pb(1)	96.1(6)	O(2)–C(8)–C(4)	119.8(9)
Pb(1)#2–O(1)–Pb(1)	118.8(3)	O(1)–C(8)–C(4)	120.6(9)
C(8)–O(2)–Pb(1)	94.4(6)	O(4)–C(9)–O(3)	124.1(10)
C(8)–O(2)–Pb(1)#1	149.8(8)	O(4)–C(9)–C(5)	115.0(11)
Pb(1)–O(2)–Pb(1)#1	110.5(3)	O(3)–C(9)–C(5)	120.9(11)
C(9)–O(3)–Pb(1)	87.5(7)		
Symmetry operation : #1 x–1/2,–y+3/2,–z+1; #2 x+1/2,–y+3/2,–z+1			

Table S3. Hydrogen bond distances for **R1** and **S1**.

Hydrogen bond distances (Å)			
Name	D–H···A	d(H···A)	d(D···A)
R1	O(5)–H(5D)···O(4)#1	1.95(8)	2.849(12)
	O(5)–H(5C)···O(3)#2	2.09	2.818(12)
	N(2)–H(2)···N(3)#3	2.09	2.859(10)
	N(5)–H(5)···O(6)#3	2.07	2.921(10)
	N(4)–H(4)···O(6)#4	2.29	2.993(10)
Symmetry operation : #1 x-1/2,-y+1/2,-z+1; #2 x+1/2,-y+1/2,-z+1; #3 -x+1,y+1/2,-z+1/2; #4 -x+1,y-1/2,-z+1/2			

Hydrogen bond distances (Å)			
Name	D–H···A	d(H···A)	d(D···A)
S1	O(5)–H(5C)···O(3)#1	1.92(5)	2.864(13)
	O(5)–H(5D)···O(4)#2	2.22(11)	2.860(13)
	N(2)–H(2)···N(3)#3	2.03	2.890(12)
	N(5)–H(5)···O(6)#3	2.09	2.952(13)
	N(4)–H(4)···O(6)#4	2.29	3.013(12)
Symmetry operation : #1 x-1/2,-y+3/2,-z+1; #2 x+1/2,-y+3/2,-z+1; #3 -x+1,y-1/2,-z+1/2; #4 -x+1,y+1/2,-z+1/2			

Table S4. Maximum adsorption capacity for CR on various adsorbents.

Adsorbents (MOFs)	q_{max} (mg g^{-1})	Surface area (m^2 g^{-1}) [a]	Ref.
[Pb((*S*,*S*)-*TBA*)(H_2O)] ·1.7H_2O	138.57	10.55	This work
Zn-TDPAT	16.72	X	[1]
Fe_3O_4@SiO_2@Zn-TDPAT	17.73	X	[1]
[Zn(BDC)(TIB)]·3H_2O	60.2	X	[2]
ZIF-8@$CoFe_2O_4$	64.48	918.9	[3]
Co-BDC (MOF-4)	64.56	0.9113	[4]
TMU-4	72	518	[5]
Cu-BDC (MOF-3)	77.05	89.9110	[4]
TMU-9	92	X	[6]
In-MOFs-2	92.29	7.3480	[7]
AlF	93.45	973.39	[8]
TMU-34	94	540	[5]
GO/In-MOFs-2	96.72	10.8585	[7]
TMU-8	97.3	X	[6]
AlF-GO	102.04	917.79	[8]
In-MOFs-1	103.54	21.1983	[7]
GO/In-MOFs-1	108.54	14.3261	[7]
SALE-TMU-34	112	720	[5]
Cu-BTC (MOF-1)	120.15	32.0708	[4]
Co-BTC (MOF-2)	129.95	7.7682	[4]
USALE-TMU-34	138	830	[5]
AlF-rGO	178.57	951.88	[8]
ZIF-67@C-MOF-74	180	753	[9]
$[Ni_2F_2(4,4'\text{-bipy})_2(H_2O)_2][VO_3]_2\cdot 8H_2O$	242.1	X	[10]
TFMOF	252.25	89.9	[11]
UiO-66	283	1358	[12]
In-TATAB	299	623	[13]
Fe_3O_4@ZTB-1	458	X	[14]
SCNU-Z1-Cl	585	1636	[15]
UiO-66-2.7Ti	607	929	[12]
Cu-BTC-b	884.96	1119.7	[16]
Ni-MOFs	2046	59.8	[17]
GO/MOF	2489	69.6	[17]

[a] X : not measured surface area.

Table S5. Zeta potential values for **S1** under the various pH conditions.

	pH 2	pH 3	pH 4	pH 7	pH 11
Zeta potential (mV)	11.5	9.34	9.11	2.59	-18.3

Table S6. pH value of aqueous H_2SO_4 solutions before and after immersion.

	H_2SO_4 pH values	
Before immersion	2.60	3.35
After immersion	3.41	3.53

The pH values of each solution were adjusted using H_2SO_4. The well ground samples for **S1** were immersed into aqueous H_2SO_4 solutions at room temperature for 24 h. We investigated the pH value of the aqueous H_2SO_4 solutions before and after immersion of **S1** at pH 2.60 and 3.35, respectively (Table S6). The pH values were measured using a pH meter.

If the pH < 3, the pH values of the H_2SO_4 supernatant are greater than that of the solution in the absence of **S1**, which might be attributed to the protonation within the framework (Table S6). The SO_4^{2-} exist as counter anions to maintain the charge balance with the acidic cationic framework. The elemental analysis and infrared spectra clearly confirm the existence of S and the stretching vibration of SO_4^{2-}, respectively, for **S1** soaked in aqueous H_2SO_4 solution (Table S7, Figure S14).[18, 19] As a result, the molecular structure of CR still exists as an anion because the pH value is higher than the isoelectric point of CR.

Table S7. Elemental analysis of **S1** and **S1** immersed in H_2SO_4.

	C	H	N	S
Calculated	20.59	3.15	13.34	-
Before immersion	20.61	2.93	13.22	-
After immersion	19.77	2.96	12.63	0.67

Figure S15. Infrared spectra for **S1** and **S1** immersed in H_2SO_4.

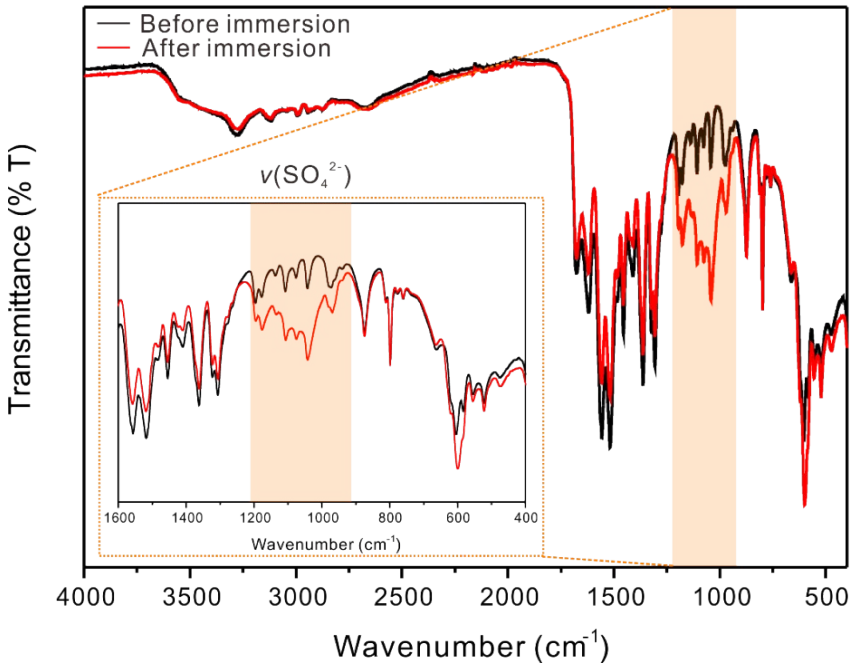

References

1. R. Wo, Q.-L. Li, C. Zhu, Y. Zhang, G.-f. Qiao, K.-y. Lei, P. Du and W. Jiang, Preparation and Characterization of Functionalized Metal–Organic Frameworks with Core/Shell Magnetic Particles (Fe_3O_4@SiO_2@MOFs) for Removal of Congo Red and Methylene Blue from Water Solution. *J. Chem. Eng.*, 2019, **64**, 2455-2463.
2. X. Zhang, Y. Gao, H. Liu and Z. Liu, Fabrication of porous metal–organic frameworks via a mixed-ligand strategy for highly selective and efficient dye adsorption in aqueous solution. *CrystEngComm*, 2015, **17**, 6037-6043.
3. Y. Xu, J. Jin, X. Li, Y. Han, H. Meng, J. Wu and X. Zhang, Rapid magnetic solid-phase extraction of Congo Red and Basic Red 2 from aqueous solution by ZIF-8@$CoFe_2O_4$ hybrid composites. *J. Sep. Sci.*, 2016, **39**, 3647-3654.
4. F.-h. Wei, D. Chen, Z. Liang, S.-q. Zhao and Y. Luo, Synthesis and characterization of metal–organic frameworks fabricated by microwave-assisted ball milling for adsorptive removal of Congo red from aqueous solutions. *RSC Adv.*, 2017, **7**, 46520-46528.
5. S. A. A. Razavi and A. Morsali, Ultrasonic-Assisted Linker Exchange (USALE): A Novel Post-Synthesis Method for Controlling the Functionality, Porosity, and Morphology of MOFs. *Chem. Eur. J.*, 2019, **25**, 10876-10885.
6. M. Y. Masoomi, A. Morsali and P. C. Junk, Rapid mechanochemical synthesis of two new Cd(ii)-based metal–organic frameworks with high removal efficiency of Congo red. *CrystEngComm*, 2015, **17**, 686-692.
7. F.-h. Wei, Q.-h. Ren, Z. Liang and D. Chen, Synthesis of Graphene Oxide/Metal-Organic Frameworks Composite Materials for Removal of Congo Red from Wastewater. *ChemistrySelect*, 2019, **4**, 5755-5762.
8. R. Azhdari, S. M. Mousavi, S. A. Hashemi, S. Bahrani and S. Ramakrishna, Decorated graphene with aluminum fumarate metal organic framework as a superior non-toxic agent for efficient removal of Congo Red dye from wastewater. *J. Environ. Chem. Eng.*, 2019, **7**, 103437.
9. M. del Rio, G. Turnes Palomino and C. Palomino Cabello, Metal–Organic Framework@Carbon Hybrid Magnetic Material as an Efficient Adsorbent for Pollutant Extraction. *ACS Appl. Mater. Interfaces*, 2020, **12**, 6419-6425.
10. J. Zolgharnein, S. Dermanaki Farahani, M. Bagtash and S. Amani, Application of a new metal-organic framework of $[Ni_2F_2(4,4'\text{-bipy})_2(H2O)_2](VO_3)_2.8H_2O$ as an efficient adsorbent for removal of Congo red dye using experimental design optimization. *Environ. Res.*, 2020, **182**, 109054.
11. J. Liu, H. Yu and L. Wang, Superior absorption capacity of tremella like ferrocene based metal-organic framework in removal of organic dye from water. *J. Hazard. Mater.*, 2020, **392**, 122274.
12. Y. Han, M. Liu, K. Li, Q. Sun, W. Zhang, C. Song, G. Zhang, Z. Conrad Zhang and X. Guo, In

situ synthesis of titanium doped hybrid metal–organic framework UiO-66 with enhanced adsorption capacity for organic dyes. *Inorg. Chem. Front.*, 2017, **4**, 1870-1880.

13. X. Liu, B. Liu, J. F. Eubank and Y. Liu, Highly effective and fast removal of anionic carcinogenic dyes via an In_3-cluster-based cationic metal–organic framework with nitrogen-rich ligand. *Mater. Chem. Front*, 2020, **4**, 182-188.
14. L.-J. Han, F.-Y. Ge, G.-H. Sun, X.-J. Gao and H.-G. Zheng, Effective adsorption of Congo red by a MOF-based magnetic material. *Dalton Trans.*, 2019, **48**, 4650-4656.
15. S.-Q. Deng, X.-J. Mo, S.-R. Zheng, X. Jin, Y. Gao, S.-L. Cai, J. Fan and W.-G. Zhang, Hydrolytically Stable Nanotubular Cationic Metal–Organic Framework for Rapid and Efficient Removal of Toxic Oxo-Anions and Dyes from Water. *Inorg. Chem.*, 2019, **58**, 2899-2909.
16. Y. Luo, D. Chen, F. Wei and Z. Liang, Synthesis of Cu-BTC Metal-Organic Framework by Ultrasonic Wave-Assisted Ball Milling with Enhanced Congo Red Removal Property. *ChemistrySelect*, 2018, **3**, 11435-11440.
17. S. Zhao, D. Chen, F. Wei, N. Chen, Z. Liang and Y. Luo, Removal of Congo red dye from aqueous solution with nickel-based metal-organic framework/graphene oxide composites prepared by ultrasonic wave-assisted ball milling. *Ultrason. Sonochem.*, 2017, **39**, 845-852.
18. X.-Y. Dong, J.-J. Li, Z. Han, P.-G. Duan, L.-K. Li and S.-Q. Zang, Tuning the functional substituent group and guest of metal–organic frameworks in hybrid membranes for improved interface compatibility and proton conduction. *J. Mater. Chem. A.*, 2017, **5**, 3464-3474.
19. G. Socrates, *Infrared and Raman characteristic group frequencies: tables and charts*, John Wiley & Sons, 2004, pp. 290-291.